INTERNATIONAL JOURNAL FOR NUMERICAL METHODS IN FLUIDS
Int. J. Numer. Meth. Fluids 2001; **35**: 763–784

Computational modelling of flow around a circular cylinder in sub-critical flow regime with various turbulence models

M. Tutar[a,*,1] and A. E. Holdø[b]

[a] *Makine Muhendisligi Bolumu, Mersin Universitesi, Ciftlikkoy, Mersin, Turkey*
[b] *Aeronautical, Civil and Mechanical Engineering Department, University of Hertfordshire, Hatfield, U.K.*

SUMMARY

The numerical simulation of transitional flow around a two-dimensional stationary circular cylinder is presented using two groups of turbulence models in a sub-critical flow regime. In the first group, enhanced two-equation turbulence models based on the eddy viscosity concept are used. They include the non-linear $k-\varepsilon$ model with extended models, such as renormalization group (RNG) and the anisotropic model. In the second group, flow simulation is carried out using the large eddy simulation (LES) method, which is based on a standard sub-grid scale (SGS) model with a near-wall approach. This near-wall model, without using the 'law of wall', is achieved in a finite element code. The numerical results extracted from these simulations are compared with each other and with the experimental data in order to determine the relative performance of these turbulence models and to find the best model for the flow of interest. Although most of the LES simulations have been previously carried out using finite volume methods, results from using the present model show that the finite element method (FEM) can also be used with confidence. Copyright © 2001 John Wiley & Sons, Ltd.

KEY WORDS: circular cylinder; finite element method; $k-\varepsilon$ based turbulence models; LES method; transitional flow

1. INTRODUCTION

One of the classical problems in fluid mechanics is the determination of the flow field around a bluff body represented by a circular or rectangular cylinder. This is of great interest in many engineering applications, such as hydrodynamic loading on ocean marine piles and offshore platform risers and support legs. The early experiments [1,2] emphasized the effect of turbulence for the cylinder flow problem with an increase in Reynolds number. The first

* Correspondence to: Makine Muhendisligi Bolumu, Mersin Universitesi, Ciftlikkoy, 33160 Mersin, Turkey. Tel.: + 90 324 3610001; fax: + 90 324 3610032.
[1] E-mail: m.tutar@mersin.edu.tr

Received November 1999
Revised June 2000

experiment shows that at a Reynolds number of 150, the vortex street becomes turbulent in the wake downstream of the cylinder and at a Reynolds number of 400, the vortices become turbulent after the separation point somewhere in the wake formation region. The second experiment, on the other hand, indicates that the transition from laminar flow to turbulent flow in the boundary layer can take place even at low Reynolds numbers and the boundaries of the flow regimes are directly affected by the change in the Reynolds number. Thus, even though the boundary layer remains laminar up to a certain Reynolds number, the computation of vortex shedding from the cylinder may require turbulence models.

Turbulence modelling is always an important consideration of computational fluid dynamics (CFD) modelling of complex flows. Numerical simulations with the standard $k-\varepsilon$ turbulence model [3] suggest that the separated turbulent flow past a cylinder cannot be predicted realistically with a steady state flow simulation ignoring the unsteady separation involving periodic motion. This is because the periodic shedding and particularly the interaction between the alternating vortices shed from the upper and lower surfaces of the cylinder appear to have a strong influence on the overall flow behaviour, and hence on the pressure forces and the drag of the cylinder. On the other hand, the study of Franke *et al.* [4], which evaluates the detailed experiments of Cantwell and Coles [5] by using transient simulations with the widely used standard linear $k-\varepsilon$ turbulence model of Launder and Spalding [6], also does not give good predictions for the resolution of flow field around the cylinder, as the model is incapable of accurately predicting turbulent flow field where the local anisotropy plays an important part.

As the standard $k-\varepsilon$ model does not perform well for near-wall predictions of high-Reynolds number flow, in order to increase the capability of this model for some cases, a variety of modified versions of the standard $k-\varepsilon$ model used with wall functions have also been proposed, among which are the non-linear $k-\varepsilon$ models, the renormalization group (RNG) based models and anisotropic eddy viscosity models. The non-linear $k-\varepsilon$ model unlike the standard one that uses the Reynolds stress, being a linear function of the strain tensor, renders the Reynolds stress tensor as a non-linear function of the strain rate tensor and provides the necessary mechanism for predicting turbulence anisotropy effects. The non-linear $k-\varepsilon$ turbulence model proposed by Speziale [7] is validated against internal flow and results indicate that such models are able to predict the anisotropy of turbulence for some cases more accurately than the standard linear form of the $k-\varepsilon$ model. Further numerical work of Rabbit [8] combines this non-linear $k-\varepsilon$ turbulence model with extended turbulence models, such as RNG for impinging jet problems, and improves the prediction of turbulence levels compared with the standard $k-\varepsilon$ turbulence model. The RNG $k-\varepsilon$ turbulence model introduces a modification of the production of dissipation terms of account for non-equilibrium strain rates and it becomes a useful enhanced two-equation turbulence model for some turbulence flow problems.

The large eddy simulation (LES) method on the other hand is introduced as a compromise between two-equation turbulence models that are based on the time-averaged Navier–Stokes equations and direct numerical simulation (DNS). These methods employ the space-averaged equations of fluid flow and arise from space averaging to Navier–Stokes equations. As the details of the LES method are much less influential for the overall flow behaviour than the time-averaged turbulence models and introduce a more universal approach to resolve the flow field, this method has begun to be employed to analyse various turbulent flow cases. Although the LES method seems to be more expensive computationally than the other approaches in

common use, initial numerical works investigating vortex shedding flow from bluff bodies show that good results can be obtained even with a small number of mesh points. The numerical studies [9,10], which include the finite volume based LES applications, prove that LES methods with a more reliable near-wall approach can replace two-equation based eddy viscosity models for the cylinder problem. In the literature most authors use finite volume based codes for LES modelling. There are also some pioneering works, including finite element simulations using LES method as found in the studies of Kato and Ikegawa [11] and Simpson *et al.* [12].

2. GOVERNING EQUATIONS FOR THE TURBULENCE MODELS

2.1. Time-averaged two-equation models

2.1.1. Standard linear k–ε model. The standard linear k–ε turbulence model is well known and the model has been tested for vortex shedding flow by Majumdar and Rodi [3] previously. The Reynolds stress tensor, τ_{ij}, which appears on the right-hand side of the time-averaged Navier–Stokes equations as a result of time averaging to Navier–stokes equations, is related to kinetic energy k and turbulent dissipation ε by a following formula:

$$\tau_{ij} = \frac{2}{3}\rho k\delta_{ij} + 2\mu_t S_{ij} \tag{1}$$

where

$$\mu_t = \rho C_\mu \frac{k^2}{\varepsilon}, \qquad S_{ij} = \frac{1}{2}\left(\frac{\partial \bar{u}_i}{\partial x_j} + \frac{\partial \bar{u}_j}{\partial x_i}\right)$$

The forms of the k and ε equation of the standard linear k–ε model are then gives as follows:

$$\frac{\mathrm{D}k}{\mathrm{D}t} = \frac{\partial}{\partial x_j}\left(\frac{v_t}{\sigma_k}\frac{\partial k}{\partial x_j}\right) + v_t\left(\frac{\partial \bar{u}_i}{\partial x_j} + \frac{\partial \bar{u}_j}{\partial x_i}\right)\frac{\partial \bar{u}_i}{\partial x_j} - \varepsilon \tag{2}$$

$$\frac{\mathrm{D}\varepsilon}{\mathrm{D}t} = \frac{\partial}{\partial x_j}\left(\frac{v_t}{\sigma_\varepsilon}\frac{\partial \varepsilon}{\partial x_j}\right) + C_1\frac{\varepsilon}{k}v_t\left(\frac{\partial \bar{u}_i}{\partial x_j} + \frac{\partial \bar{u}_j}{\partial x_i}\right)\frac{\partial \bar{u}_i}{\partial x_j} - C_2\frac{\varepsilon^2}{k} \tag{3}$$

The coefficients C_1, C_2, C_μ, σ_k, σ_ε are constants in the sense that they are not changed in any calculation. However, these constants need to be changed in order to accommodate the effects such as low *Re*, near wall, etc.

2.1.2. Non-linear RNG k–ε model. The RNG k–ε model employed in the present finite element code [3] is that developed by Yakhot *et al.* [14]. This model is very similar in form to the standard and extended k–ε turbulence models; however, the RNG k–ε model differs from the standard model by the inclusion of an additional sink term in the turbulence dissipation equation to account for non-equilibrium strain rates and employs different values for the

various model coefficients. The form of the k equation remains same. The turbulence dissipation ε equation of the RNG k–ε model includes the following sink term:

$$\frac{C_\mu \eta^3 (1-\eta/\eta_0)}{1+\beta\eta^3}\frac{\varepsilon^2}{k} \tag{4}$$

In the above term the extra term employs the parameter η, which is the ratio between the characteristic time scales of turbulence and the mean flow field as follows:

$$\eta = S\frac{k}{\varepsilon}$$

where

$$S = \sqrt{2S_{ij}S_{ij}} = \sqrt{G/\mu_t}$$

The primary model coefficients of the RNG k–ε turbulence model are C_μ, C_1, C_2, σ_k, σ_ε and the von Karman constant, κ. Yakhot *et al.* [4] recommend the values of these model coefficients as in Table I.

2.1.3. The anisotropic k–ε turbulence model. This model is the version of the standard k–ε turbulence model that includes terms in the turbulence dissipation equation that relate to the anisotropic structure of the turbulence field. The form of the kinetic energy and turbulence dissipation of the anisotropic k–ε model is identical to that of the standard k–ε model. The difference is the way in which the model parameters C_1 and C_2 are obtained, as follows:

$$C_1 = 1.125 \text{ Launder's model;} \qquad C_2 = \frac{1.92}{(1+0.9A^{1/2}A_2)}$$

where

$$A \equiv 1 - \frac{9}{8}(A_2 - A_3)$$

$$A_2 = a_{ij}a_{ij}, \quad \text{second invariant of } a_{ij}$$

$$A_3 = a_{ij}a_{jk}a_{ki}, \quad \text{third invariant of } a_{ij}$$

Table I. Sets of values used for RNG k–ε turbulence model.

C_μ	C_1	C_2	σ_k	σ_ε	κ
0.085	1.41	1.68	0.7179	0.7179	0.3875

$$a_{ij} = \left(\frac{\overline{u_i' u_j'}}{k} - \frac{2}{3}\delta_{ij} \right), \quad \text{the anisotropy tensor}$$

As can be seen above, the model constant C_2 depends on the anisotropy tensor a_{ij}, which is derived from the Reynolds stress tensor.

In the present study the Boussinesq eddy viscosity model that ensures the Reynolds stress to be a linear function of the strain rate tensor is not used. The Reynolds stress tensor, however, is obtained from Launder's anisotropic eddy viscosity model [15] and is combined with the RNG k–ε. Launder's model renders the Reynolds stress tensor a cubic function of the strain tensor and is believed to be better equipped to predict some types of recirculating flows.

2.2. The sub-grid scale stress model

In the present work, as an alternative approach to the two-equation based time-averaged turbulence models, a space-averaged turbulence model, a sub-grid scale (SGS) stress model, is used. This model, or LES method, by introducing a space averaging technique into the Navier–Stokes equations directly solves scales larger than the mesh size, while modelling smaller scales in the flow domain. For turbulent flow computations, space-averaged Navier–Stokes equations of motion of an incompressible fluid can be written as follows:

$$\frac{\partial \hat{u}_i}{\partial t} + \frac{\partial}{\partial x_j}\hat{u}_i\hat{u}_j = -\frac{1}{\rho}\frac{\partial P}{\partial x_i} + \frac{\partial}{\partial x_j}\left[v\left(\frac{\partial \hat{u}_i}{\partial x_j} + \frac{\partial \hat{u}_j}{\partial x_i} - \tau_{ij} \right) \right] + b_i \tag{5}$$

$$\frac{\partial \hat{u}_i}{\partial x_i} = 0 \tag{6}$$

The term τ_{ij} in the space-averaged equation (5) is called the SGS stress term and is represented by an SGS eddy viscosity model as

$$\tau_{ij} = -v_t\left(\frac{\partial \hat{u}_i}{\partial x_j} + \frac{\partial \hat{u}_j}{\partial x_i} \right) \tag{7}$$

In the above equations, the SGS eddy viscosity term, v_t, can be obtained by analogy with the commonly used eddy viscosity models for the Reynolds stress. Since v_t is dimensionally L^2T^{-1}, and a natural length scale for small scale eddies is provided by the width of the filter, Δ, there is only a time scale required and the natural choice is a velocity derivative. This leads to the strain model, which is initially derived by Smagorinsky [16] as

$$v_t = (C_s\Delta)^2(\hat{S}_{ij}\hat{S}_{ij})^{1/2} \tag{8}$$

This model is generally known as SGS Model of Smagorinsky. The first term on the right-hand side of Equation (8), the Smagorinsky constant C_s, can be chosen in a range from 0.10 to 0.30 and it is required to have a sensible value to avoid excessive damping of resolved structures. The second term, the grid size Δ, as an indication of characteristic length scale separates large and small scale eddies from each other and is considered to be an average cell

size. It is calculated for two-dimensional elements in the present finite element method (FEM) code as follows:

$$\Delta = f(\Delta x \Delta y)^{1/2} \tag{9}$$

The third term on the other hand is the resolvable strain rate and can also be given as follows:

$$\hat{S}_{ij} = \frac{1}{2}\left(\frac{\partial \hat{u}_i}{\partial x_j} + \frac{\partial \hat{u}_j}{\partial x_i}\right) \tag{10}$$

The SGS eddy viscosity in the present FEM code is obtained by analogy with the commonly used eddy viscosity based mixing length model of Prandtl [17].

3. COMPUTATIONAL PRINCIPLES

3.1. Numerical approach

All simulations have been carried out using a commercial code [13], which is based on the FEM. In the FEM code the whole flow region is subdivided into a finite number of small two-dimensional four-noded quadrilateral elements called finite elements. The partial differential equations (PDEs) of fluid mechanics covering the flow region as a whole are replaced by ordinary differential equations (ODEs) or algebraic equations in each element. The resulting system of non-linear equations is then solved by a segregated solution algorithm with a second-order trapezoid time integration scheme.

3.2. Computational domain and boundary conditions

The geometric size of the computational domain and the boundary conditions imposed for all simulations are shown in Figure 1. The cylinder has a non-dimensional unit diameter and is situated in the centre of the vertical plane. Inlet (upstream), upper and lower boundaries have been extended in the lateral direction so that the effects due to the cylinder presence have been assumed to be negligible at these boundaries. The domain has been also extended long enough downstream to eliminate the far field effects on the near wake and to produce full development of the vortex street. The velocity boundary and initial conditions used for all numerical simulations have been as follows:

(i) no-slip conditions on the cylinder surface ($u = v = 0$)
(ii) uniform flow at the inlet and upper and lower boundaries ($u = U$, $v = 0$)
(iii) one cycle initial sinusoidal velocity boundary condition in the y-direction at the inlet ($v = v_m \text{ Sin } 2\pi ft$)
(iv) free outflow condition

Uniform, non-dimensional upstream velocity has been used while the non-dimensional velocity amplitude (v_m/U) and the non-dimensional frequency (fD/U) have been set to 0.0329

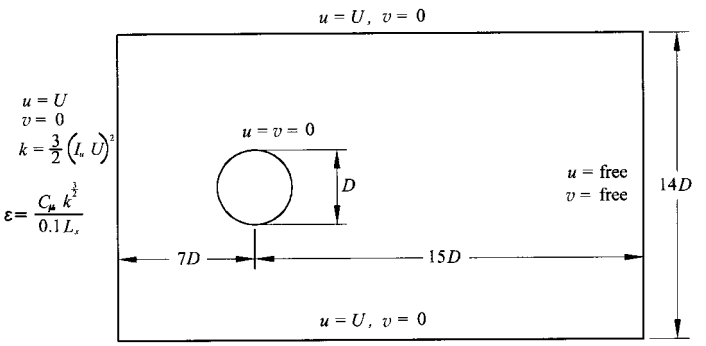

Figure 1. The geometric size of the computational domain and the boundary conditions imposed (the initial conditions for k and ε are not imposed for LES).

and 0.0238 respectively. Apart from initial and boundary conditions for velocity components, for the $k-\varepsilon$ based turbulent models only the free stream inlet turbulence values for kinetic energy and turbulent dissipation have been also imposed based on a turbulent intensity (I_u) of 0.6 per cent and a non-dimensional turbulent length scale (L_x/D) of 0.02. The calculations have been carried out with a non-uniformly spaced numerical grid for eddy viscosity based two-equation models with 11474 nodes, and for the LES simulations with 21864 and 34804 nodes respectively. The mesh size has been increased with the distance from the cylinder surface, and the distance of the first grid point from the cylinder wall has been chosen to be 0.8 per cent of the cylinder diameter for the first group turbulence models and 0.2 per cent for the LES simulation due to the differing wall formulation approaches for these two different groups of turbulence models. Figure 2 shows the computational mesh used for LES simulation with 21864 nodes.

3.3. Near-wall treatment

For the first group of turbulence models in the near-wall region, a near-wall modelling methodology that combines the law of the wall approach with van Driest's mixing length approach has been used [18].

For the LES simulations, no wall function has been used but wall effects have been taken into consideration by reducing the length scale $l = C_s\Delta$ in the vicinity of the cylinder wall up to some distance from the cylinder wall, where the effects on the turbulence become negligible. The reason why wall functions have not been used in the present work is due to the fact that a recent review by Rodi *et al.* [19], presenting the results of a workshop on LES simulation of flow past a stationary cylinder, reveals that simulations that use of 'law of wall' boundary conditions do not seem to be reliable enough to be used with confidence in separated flows, and the best treatment will be to use a sufficiently fine mesh to resolve the near-wall flow with no-slip condition.

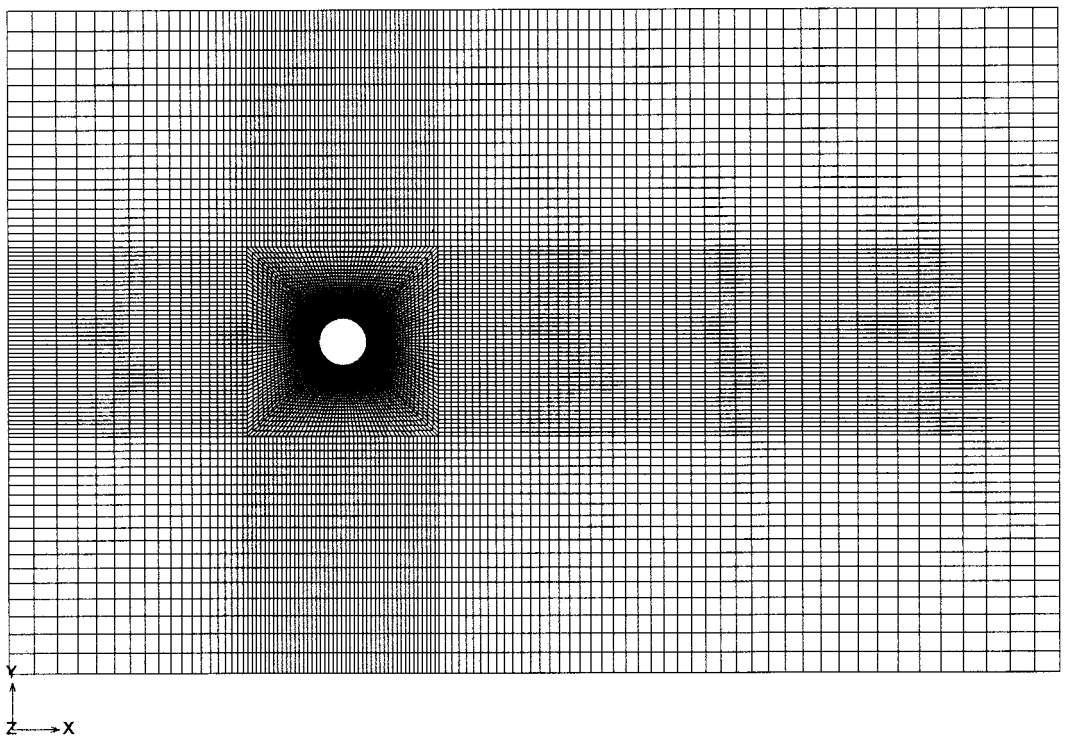

Figure 2. The computational mesh used for LES simulation with 34804 nodes.

A damping function D_T has then been introduced to reduce the length scale up to 8 per cent of the cylinder diameter and has been calculated by an alternative form of van Driest's [20] functions as follows:

$$D_T = 1 - \exp\left[-\left(\frac{y^+}{A^+}\right)^2 \right] \tag{11}$$

where A^+ is a constant for which a value of 25 is used. The above formula has the property of yielding not only $l = 0$, but also $\partial l/\partial y = 0$ on the wall. This may be preferable for numerical reasons (e.g. to avoid sharp gradients of l). Thus, by taking wall effects into account the wall region with $l = C_s \Delta D_T$, C_s has been chosen to be 0.15 for all simulations.

4. SIMULATION RESULTS AND DISCUSSIONS

All group simulations have been performed at $Re = 1.4 \times 10^5$ in the sub-critical flow regime in order to compare the results obtained with the experimental study of Cantwell and Coles [5]. All the transient simulations are summarized in Table II. The results of all two-equation k–ε based turbulence models have been presented for a free stream turbulence level of 0.6 per cent to match the value of the experimental data above. The $Re = 1.4 \times 10^5$ indicates approximately the beginning of the critical flow regime as suggested by Achenbach [2]. In this flow regime, the boundary layer all along the cylinder surface remains laminar up to and after the separation point and becomes turbulent somewhere in the free shear layer region. For this reason, simulations have needed to be carried out with turbulence models. However, the transition is not calculated by these models as they assume all turbulent flow.

Critical flow parameters, which are non-dimensional vortex shedding frequency, time-averaged drag coefficient and fluctuating lift coefficient, have been predicted with each turbulence model and their calculated values are illustrated in Table III.

Results in terms of time-averaged pressure distribution from simulations using these turbulence models are compared with each other and with the experimental data in Figure 3. It is seen that all the time-averaged pressure results on the upstream cylinder half agree well with each other. However, on the downstream cylinder half, where the boundary layer separation takes place, the calculated time-averaged pressure coefficients of all model simulations deviate from each other and from the experiment data and they give different base

Table II. Summary of turbulence models tested against a stationary cylinder in a uniform flow notation.

Re	Turbulence model	Comments
1.4×10^5	SKEM	Boussinesq eddy viscosity model
1.4×10^5	AKEM	Launder's model
1.4×10^5	RNGKEM	Launder's model
1.4×10^5	LES	LES method based on standard Smagorinsky SGS model

SKEM, standard linear k–ε model; AKEM, anisotropic non-linear k–ε model of Launder's; RNGKEM, RNG non-linear k–ε model of Launder's; LES, large eddy simulation based on SGS model.

Table III. Flow parameter results obtained from turbulence simulations for a stationary circular cylinder in a uniform flow at $Re = 1.4 \times 10^5$.

Turbulence model	St_v	$\bar{C}_D$	$\tilde{C}_L$
Standard linear k–ε	No	0.71	No
Anisotropic non-linear k–ε	0.161	0.82	0.25
RNG non-linear k–ε	0.167	0.98	0.51
LES with 21 864 nodes	0.192	1.47	0.72
LES with 34 804 nodes	0.184	1.40	0.65
Experimental of Cantwell and Coles [5]	0.179	1.237	—

All k–ε based turbulence models include 11 474 nodes.

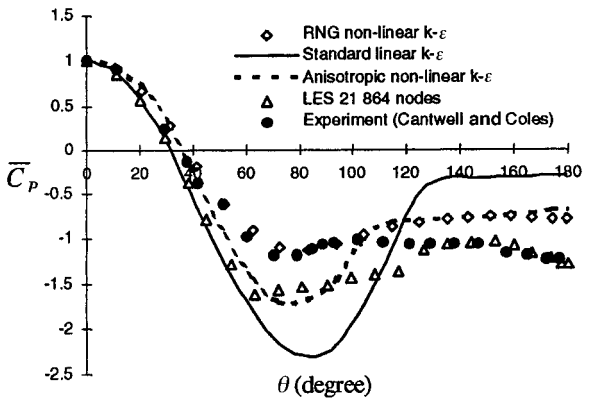

Figure 3. Time-averaged pressure distribution ($\bar{C}_P$) around a stationary circular cylinder in a uniform flow for all turbulence model simulations and experimental data of Cantwell and Coles [5] at $Re = 1.4 \times 10^5$. All k–ε based models include 11474 nodes.

pressure values. The calculated time-averaged base pressure values for the standard linear k–ε, anisotropic non-linear k–ε, and non-linear RNG k–ε models are -0.30, -0.80 and -0.72 respectively, and all of them are higher than the experimental value of -1.21. The higher time-averaged base pressure values predicted by these models causes the cylinder to experience less pressure forces leading of lower drag coefficients than the experimental value as shown in Table III. On the other hand, the LES simulation with 21 864 nodes gives an 11 per cent lower time-averaged base pressure coefficient (-1.31) than the experimental value, and a 20 per cent higher drag coefficient (1.47) than the experimental time-averaged drag prediction (1.237).

The St_v for each turbulence model has been predicted by using a power spectrum of a flow variable at a pre-selected point in the near-wake region of the cylinder. Figure 4 shows the power spectrum of the y-component velocity (UY) at a point $P\ (x, y) = (9D, 7D)$ in the near-wake region. It is seen that all turbulence models apart from the standard linear k–ε model show one dominant peak corresponding to St_v. The standard linear k–ε model does not give the sign of periodic vortex shedding motion. On the other hand, the RNG non-linear k–ε, the anisotropic non-linear k–ε turbulence models and the LES method are able to predict the vortex shedding motion with different accuracy. They give 1.167, 0.161 and 0.192 St_v values respectively. The LES simulation gives much higher momentum exchange than the enhanced k–ε based turbulence models and this higher momentum exchange for the LES method associates with a much stronger periodic vortex shedding motion compared with one for the enhanced k–ε based turbulence models, as seen in Figure 5. These predicted results are still found to be less than the experimental data. While enhanced k–ε based turbulence models yield low vortex shedding frequency, the LES method improves its prediction and gives 7.2 per cent higher St_v value than the experimental value [5] of 0.1789; the difference in St_v indicates that the modelling of turbulence with different models affects St_v.

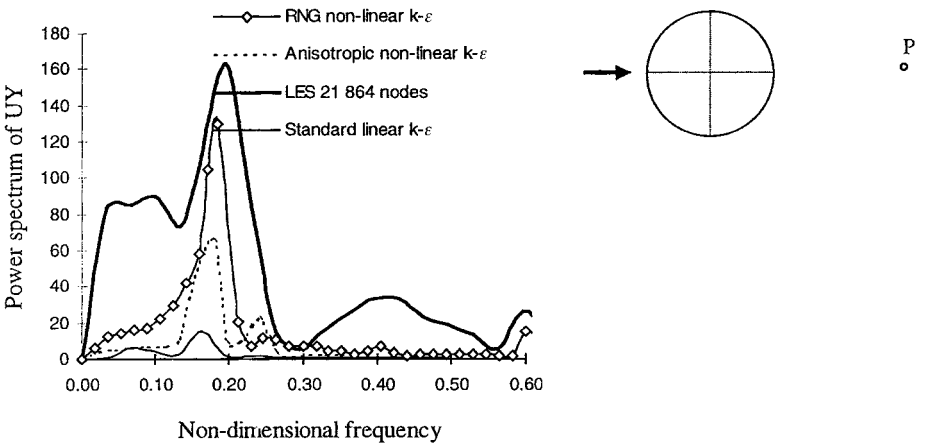

Figure 4. Power spectrum of y-component velocity (UY) for all turbulence model simulations at a point $(x, y) = (9D, 7D)$ in a near wake of the cylinder. All $k-\varepsilon$ based models include 11474 nodes.

Figure 6 displays the distribution of the time-averaged x-component velocity along the centreline of the cylinder for all simulations and gives information about the time-averaged recirculation length behind the cylinder. Experimental data [5] are also included for comparison. The standard linear $k-\varepsilon$ turbulence model gives the longest time-averaged separation zone, indicating that this turbulence model is not capable of predicting periodic fluctuations, which are associated with the vortex movement in that region. On the other hand, both RNG non-linear $k-\varepsilon$ and anisotropic non-linear $k-\varepsilon$ turbulence model simulations give shorter time-averaged separation zones with an indication of better agreement with experimental measurements [5] compared with the standard linear $k-\varepsilon$ turbulence model. Unlike the near-field centreline velocity predictions, all models give almost similar predictions for the far field. The LES method, with the introduction of the reduced turbulence length scale in the presence of the wall, effective at a distance up to 2 per cent of the cylinder diameter, shows further improvement in the predicted time-averaged separation zone, which is found to be shorter than those obtained from the other $k-\varepsilon$ based enhanced turbulence models. This shorter separation zone prediction agrees better with the experimental measurement. It also gives an indication for the reason of the slight overprediction of the St_v value of the experimental data.

The mesh resolution and the range of application of the near-wall damping term (D_T) to calculate the SGS viscosity plays a major role in obtaining different flow parameter results in the LES application. Two different grid distributions with different ranges of damping terms have been also investigated through the further calculation of the x-component velocity, as seen in Figure 7. When the number of grid-points has been increased from 21864 nodes to 34804 nodes with the damping term (D_T) introduced up to 2 per cent of the cylinder diameter, the time-averaged recirculation length increases with the decreasing effective viscosity of the system from the experimental study [5], and since the eddy viscosity itself has not been lower

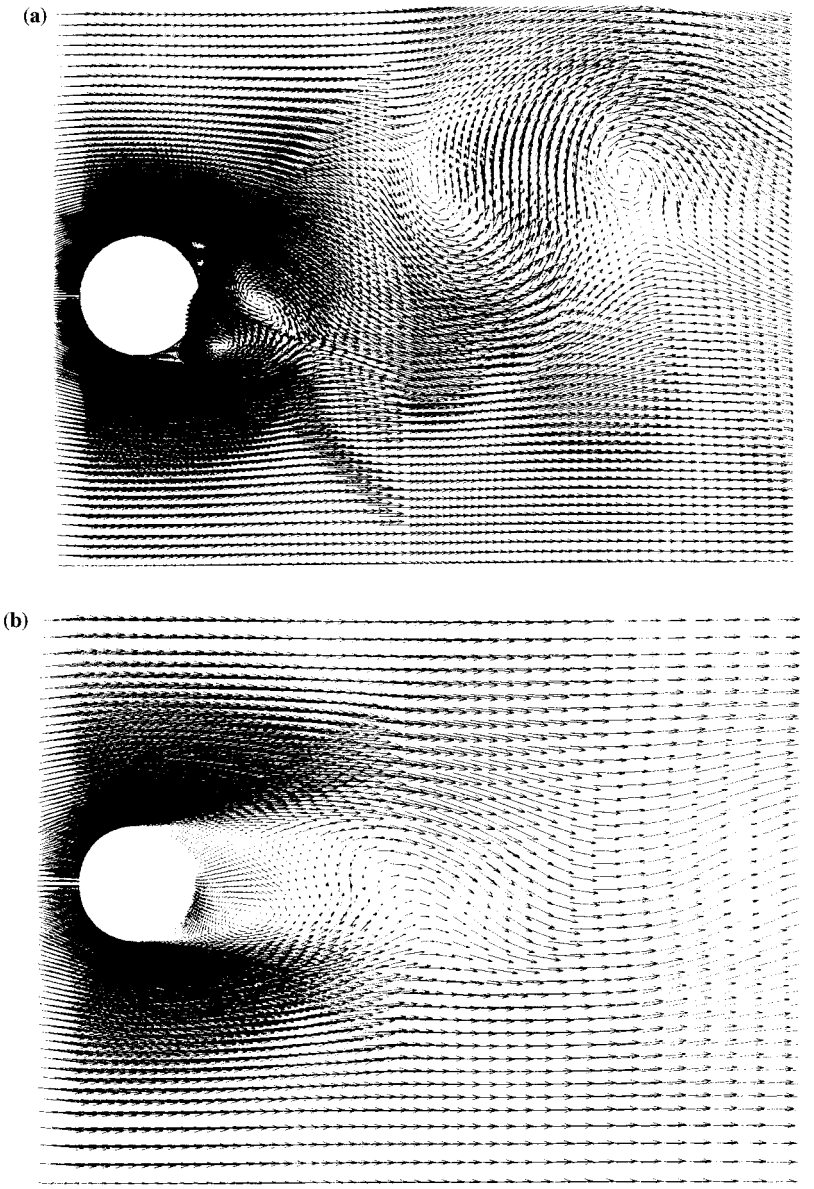

Figure 5. Velocity vector fields obtained from turbulence model simulations at a non-dimensional time of $(Ut/D) = 22.5$: (a) LES simulation; (b) RNG non-linear k–ε model.

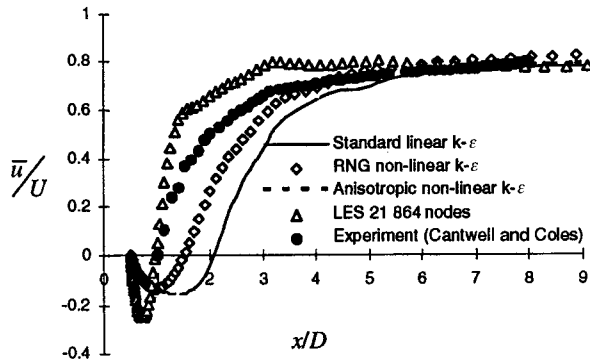

Figure 6. Time-averaged velocity distribution ($\bar{u}/U$) along the centreline of the cylinder for all turbulence model simulations and experimental data of Cantwell and Coles [5]. All k–ε based turbulence models include 11474 nodes.

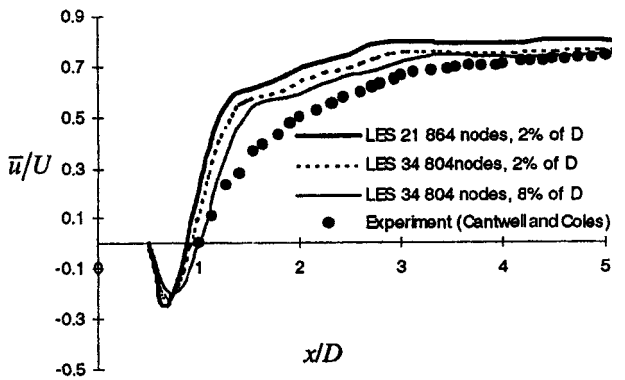

Figure 7. Time-averaged velocity distribution along the centreline of the cylinder for LES simulations containing different mesh resolutions and application range of damping term.

in the 21864 nods system calculation, the lower time-averaged recirculation length prediction for the finer mesh system may be due to two possible reasons. The first one is directly related to the present LES method application. From the definition of the present LES method, which is based on the Smagorinsky SGS model, it is known that the SGS viscosity (v_t) is proportional to $(C_s\Delta)^2$. Since the finer mesh system uses smaller grid size, it is expected to produce a lower SGS viscosity than the coarser mesh system under the same flow conditions. The second reason may be due to the numerical diffusion, which has been produced less in the finer mesh system. Hence, the lower numerical diffusion in the 34804 nodes system explains the longer time-averaged recirculation length. Further increase in the application range of the damping term from 2 to 8 per cent of the cylinder diameter also improves the prediction of the velocity

distribution. This clearly indicates that the turbulence length scale l is not only required to be reduced in the boundary layer but also in the near-wall separated region for the present two-dimensional LES simulation. The increase in the mesh resolution can also lead to more accurate predictions and ensures avoidance of the higher numerical diffusion problems. In Figure 8 the turbulence levels obtained from two mesh resolutions are compared with experimental data [5]. Because of this, the 34804 nodes mesh system gives better agreement with the experimental data as it suffers from lower numerical diffusion and produces lower v_t.

The boundary layer development and the location of the separation point for the RNG non-linear k–ε turbulence model and LES simulations are illustrated in Figure 9(a) and (b) at a non-dimensional time (Ut/D) of 7.9. In Figure 9(a) the separation angle predicted by the LES simulation is 82°, while its prediction by the RNG non-linear k–ε model simulation is 104° in Figure 9(b) at the same Ut/D. The separation point for both turbulence model simulations shows oscillatory behaviour and its position changes from $\theta_{\min} = 74°$ to $\theta_{\max} = 93°$ for the LES simulation and from $\theta_{\min} = 97°$ to $\theta_{\max} = 109°$ for the RNG non-linear k–ε model. The time-averaged separation angles for the LES method and the RNG non-linear k–ε model on the other hand are 83° and 103° respectively, while it is determined to be 77° in the experiment.

Figure 10 shows the velocity vectors in the near field of the cylinder. As can easily seen from Figure 10(a), the LES simulation shows the existence of secondary eddies, previously observed experimentally by Bouard and Coutanceau [21], unlike the k–ε based models which fail to produce them at the early stage of the wake development behind the cylinder. The further increase in the mesh density from 11474 nodes to 21864 nodes for RNG non-linear k–ε model still does not enhance the capability of this turbulence model in order to capture secondary eddies in the free shear layer, as seen in Figure 10(b). These small scale eddies play a major role in the determination of turbulence levels and the transition to turbulence in the separated

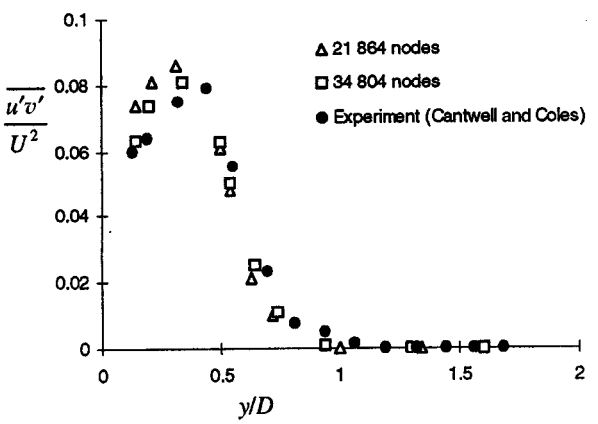

Figure 8. The comparison of global time averaged shear stress ($\overline{u'v'}/U^2$) distribution for LES simulations with different mesh resolution and experimental data of Cantwell and Coles [5] due to turbulence at $x/D = 1.0$ for the circular cylinder.

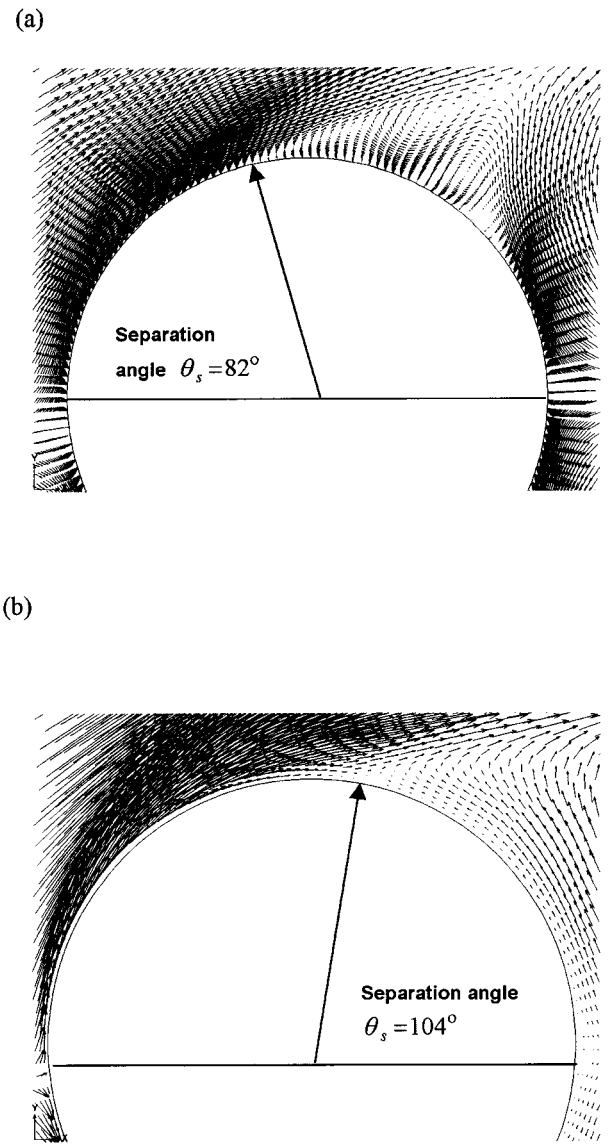

Figure 9. Velocity vector fields along the cylinder surface at a non-dimensional time $(Ut/D) = 7.9$: (a) LES simulation with 21864 nodes; (b) RNG non-linear $k-\varepsilon$ turbulence model with 11474 nodes.

region, so that their calculation becomes very important in the present model. The secondary eddies move towards the primary ones to form larger eddies as the flow develops. This strengthens the vortex formation mechanism behind the cylinder and perhaps causes a slight overprediction of the periodic vortex shedding for the LES simulations.

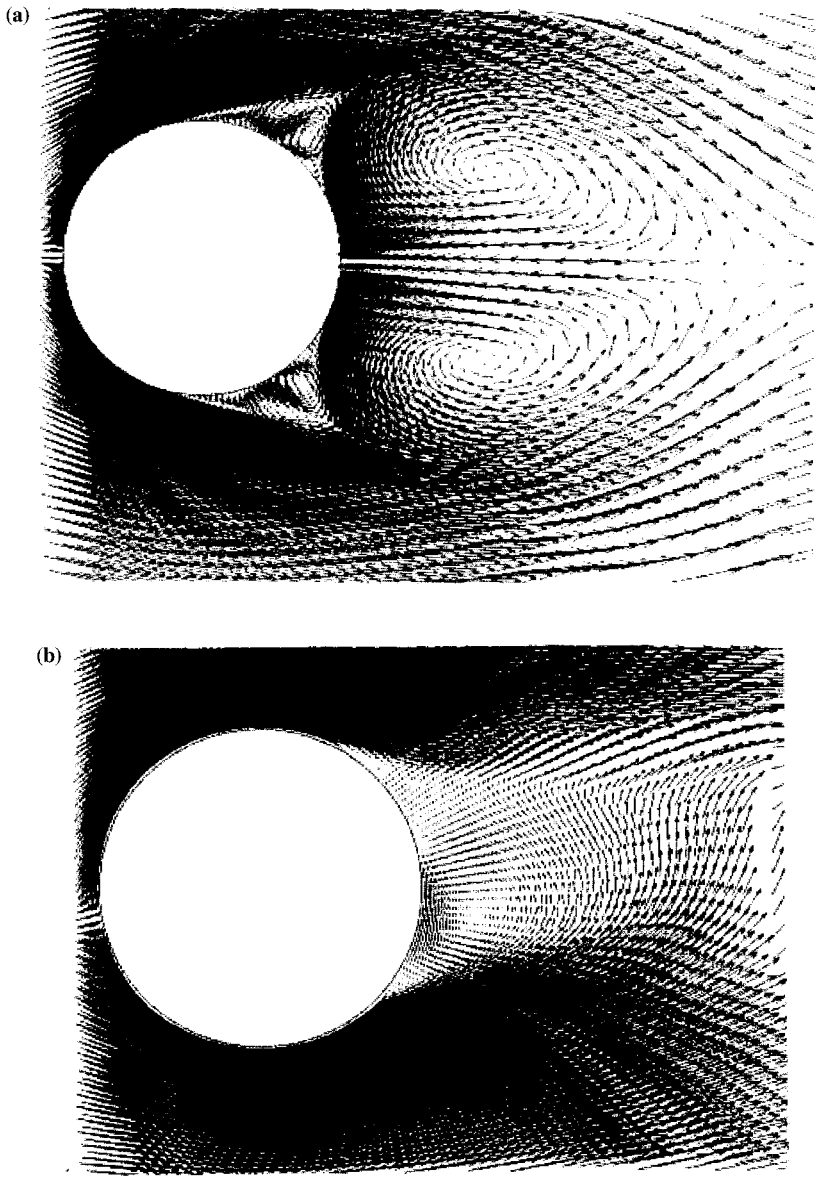

Figure 10. Velocity vector fields in a near field of the cylinder in a uniform flow at a non-dimensional time $(Ut/D) = 4.5$: (a) LES simulation with 21 864 nodes; (b) RNG non-linear $k-\varepsilon$ turbulence model with 21 864 nodes.

Vorticity plots of each model simulations are shown in Figure 11(a)–(c). All figures represent the vorticity contours at the same Ut/D of 33 for a comparison. The two non-linear enhanced $k-\varepsilon$ turbulence models are able predict vortex shedding motion and produce a periodic vortex street, including several vortices being shed asymmetrically from the cylinder (Figure 11(a) and (b)). The main difference between non-linear $k-\varepsilon$ turbulence models and the

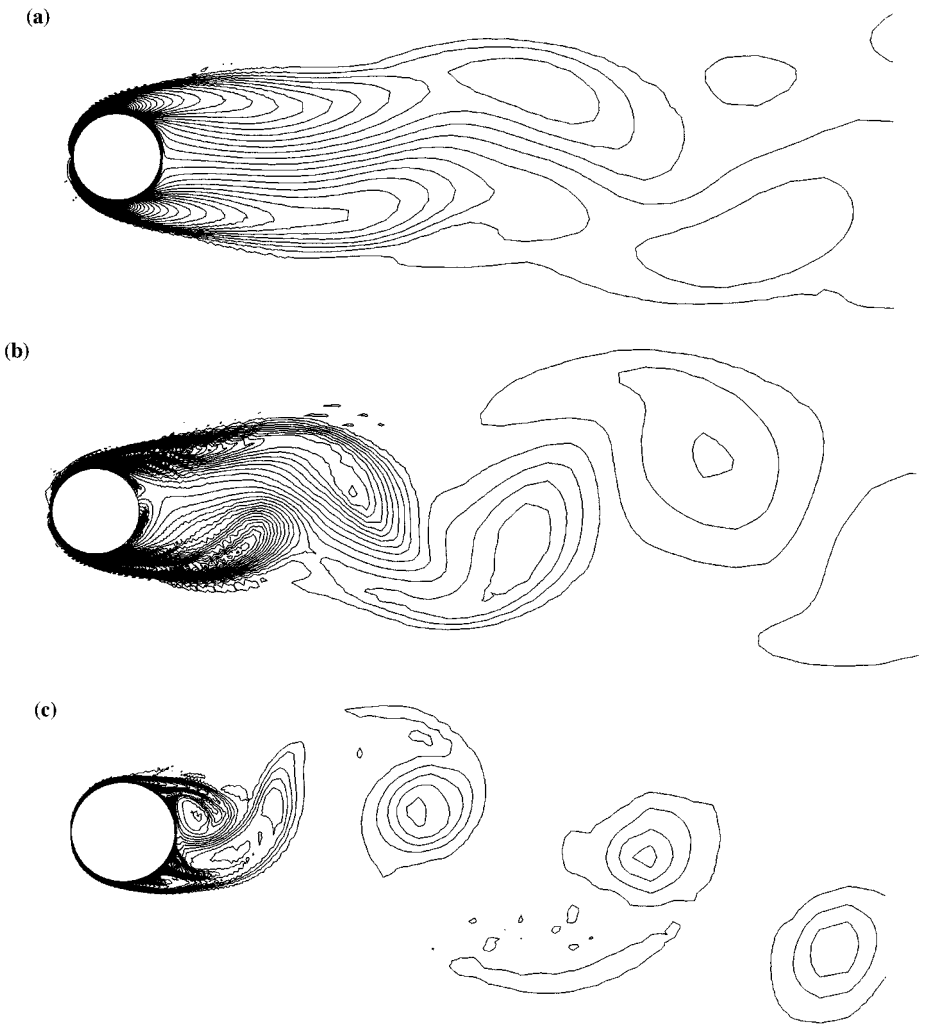

Figure 11. Instantaneous vorticity contours taken at a same contour value for two-dimensional turbulence model simulations for the cylinder. The non-dimensional time $(Ut/D) = 33$: (a) anisotropic non-linear $k-\varepsilon$ turbulence model with 11474 nodes; $\omega_{\min} = -384$ nodes, $\omega_{\max} = +396$; (b) RNG non-linear linear $k-\varepsilon$ turbulence model with 11474 nodes; $\omega_{\min} = -471$ nodes, $\omega_{\min} = +489$; (c) LES simulation with 21864 nodes, $\omega_{\min} = -576$ nodes, $\omega_{\min} = +602$.

standard linear $k-\varepsilon$ turbulence model is due to the additional non-linear terms in the equation of Reynolds stress. These non-linear terms provide a better mechanism for predicting turbulence anisotropic effects and give rise to a periodic vortex shedding motion that is not observed by the standard linear $k-\varepsilon$ turbulence model. However, the increase in the mesh density does not change the overall performances of these models in order to resolve the near flow physics but ensures slightly better flow parameter predictions as indicated in Table III. Figure 11(c) on the other hand represents the vorticity plot for the LES simulation at the same Ut/D. The strength of the vortices is greater for this simulation and they are less elongated in the streamwise direction compared with vortices obtained from other models. Stronger vortices obtained from the LES simulation thus leads this method to slightly overpredict vortex shedding motion.

The computer efficiency of the different turbulence models has also been investigated as shown in Table IV. On an IBM 6000, the calculation time to cover one vortex shedding period of the experimental data has been 10.15 h for the standard linear $k-\varepsilon$ turbulence model, 13.75 h for the anisotropic non-linear $k-\varepsilon$ turbulence model and 15.2 h for the RNG non-linear $k-\varepsilon$ turbulence model. All two-equation based $k-\varepsilon$ turbulence models have had 11474 nodes. When the mesh density was increased from 11474 nodes to 21864 nodes for the RNG non-linear $k-\varepsilon$ turbulence model, the calculation time was 30.3 h. The calculation time for LES simulations was also determined and it was 28 h for the simulation with 21864 nodes and 43 h for the simulation with 34804 nodes.

Overall results obtained from all models show that the prediction of the critical flow parameters mainly depends on the accurate calculation of the separation angle and the resolution of the flow in the separated flow region as the flow is transitional at $Re = 1.4 \times 10^5$ in that region. The more accurate prediction of the time-averaged position of separation point by the LES simulation compared with the enhanced two-equation models suggests that the LES method resolves the boundary layer better than these models and hence gives a more accurate physical picture of the flow in the free shear layer. Since the two-equation based enhanced models are based on high Re flow, and the actual boundary layer up to a separation point and afterwards somewhere in the free shear layer is still laminar at $Re = 1.4 \times 10^5$, these models do not give good predictions neither for the very near-wall flow resolution nor for the free shear layer flow. The LES method, on the other hand, by including a Van Driest-type

Table IV. Comparison of computer calculation times on an IBM 6000 computer over one vortex shedding period for all turbulence simulations.

Turbulence model	Mesh resolution (nodes)	Calculation time (h)
Standard linear k–ε	11 474	10.15
Anisotropic non-linear k–ε	11 474	13.75
RNG non-linear k–ε	11 474	15.2
	21 864	30.5
LES based on SGS model	21 864	28
	34 804	43

Cylinder is a stationary in a uniform flow at $Re = 1.4 \times 10^5$.

damping function ensures that the laminar boundary layer is better calculated in this region. The enhanced two-equation based models at this *Re* also produce too high upstream turbulent kinetic energy production leading to inadequate prediction of separation point (located towards downstream stagnation point) and a narrower wake width behind the cylinder, as seen in Figure 10(b). This causes higher base pressure, and as a result, lower time-averaged drag coefficient over the cylinder than the experimental measurements. Even though enhanced $k-\varepsilon$ based turbulence models show more improvement in the prediction of the calculation of flow parameters due to the additional non-linear terms that account for the anisotropic structure of the flow of interest, these models still are incapable of accurately predicting the flow physics, such as the accurate determination of the separation point of the flow in the free shear layers. These models do not predict the vortex shedding fluctuations accurately and give underestimated critical flow parameter results. The increase in the mesh density slightly improves the results obtained from RNG non-linear $k-\varepsilon$ model, but this model does not accommodate any improvement to accurately capture the flow physics, such as the small scale structures in the wall proximity. This fact may highlight the drawbacks of time-averaged two-equation models. The choice of the first point location from the wall on the resolution of the near wall flow and the use of 'law of wall' approach also restricts the success of the current enhanced $k-\varepsilon$ turbulence models.

The present LES method, which is based on the SGS model, resolves the boundary layer well and gives a good time-averaged separation angle, but it does not function very well in the separated region where the vortex shedding and turbulence transition take place. Since the model is designed only to model the smallest scale of eddies in the flow compared with the $k-\varepsilon$ based turbulence models, which are designed to model all scales of eddies in the flow, it has needed more grid nodes to resolve the eddies relatively larger than the grid size. For this reason, the model treats the cylinder wall regions with a much better prediction of the flow physics, such as accurate simulation of the time-averaged separation angle and production of secondary eddies, which were previously observed in experimental studies in the separated flow regions. The model predictions for the flow parameters become more realistic compared with the $k-\varepsilon$ based enhanced turbulence models, but the resolution of the local turbulent characteristics poses a challenge for the LES method, since it does not function very well in simulating turbulent quantities in the free shear layer and the wake region. The model probably introduces too much viscous energy dissipation too quickly and gives a large turbulent viscosity, as seen in Figure 8 as an indication of high turbulence level before the transition occurs in the free shear layers. However, the real flow physics as demonstrated by Achenbach [2] and later by Cantwell and Coles [5] at the sub-critical *Re* range does not show too much turbulence in the flow in the separated near-wall region. The excessive prediction in the turbulence earlier for the LES simulation leads to a considerable decrease in the vortex formation length prediction, resulting in more compact and stronger vortices being carried away from the cylinder and breaking into smaller eddies in a shorter period of time compared with other models. It is also possible that numerical diffusion arising due to application of a upwinding scheme, which is used to stabilize the numerical solution, may contribute to the underprediction of the time-averaged recirculation length and hence the overprediction of the flow parameter predictions. Both higher mesh resolution and the near-wall approach introducing a damping term into the calculation of turbulent length scale in the separated region, a well

as in the boundary layer, seem to improve the flow resolution in the near field region, as seen in Figures 7 and 8, but the current SGS model still needs further refinement to overcome the problem associated with the transitional behaviour of the flow in that region.

5. CONCLUDING REMARKS

The use of enhanced two-equation k–ε turbulence models with non-linear terms seems to improve the capability of the standard k–ε turbulence model to predict the vortex shedding flow more accurately than the standard linear model, but enhanced models still have some problems in predicting this highly time-dependent phenomenon as they are designed for flows that are steady in mean. On the other hand, LES methods with the SGS model yield much more realistic pictures for the vortex shedding flow in this transitional flow regime, but produce slightly overestimated critical flow parameter results. This may be because the turbulence is a vortex stretching process, which takes place in three dimensions and two-dimensional LES methods do not entirely capture this vortex stretching process. Apart from this, as explained above, the LES method does not account for the transitional behaviour of the flow in the sub-critical flow, regime as it produces high energy dissipation too early. LES based models require a reduction in the eddy viscosity produced by the Smagorinsky model in the separated region. In this case, a new model could be development to reduce the viscous dissipation in the near field. Good mesh resolution in that region and selection of length scale can also improve the capability of this model in two-dimensional calculations. The present method also shows the applicability of the SGS model by using the FEM for the calculation of vortex shedding flow.

ACKNOWLEDGMENTS

The authors acknowledge the support of Mersin University and the Computational Fluid Dynamics Group at the University of Hertfordshire for their help and financial support.

APPENDIX A. NOMENCLATURE

b_i	body force term
$\bar{C}_{\mathrm{D}}$	time-averaged drag coefficient
$\tilde{C}_{\mathrm{L}}$	periodic lift coefficient
C_1	empirical constant
C_2	empirical constant
C_μ	empirical constant
C_s	Smagorinsky constant
D	cylinder diameter
D_T	damping term
f	vortex shedding frequency
G	generation of turbulence kinetic energy
k	turbulent kinetic energy

I_u	turbulent scale
l	length scale
p	pressure
Re	Reynolds number
S_{ij}	strain rate tensor
$\bar{S}_{ij}$	resolvable strain rate
St_v	non-dimensional vortex shedding frequency
t	time
u	x-component velocity
U	free stream velocity
u_i	u, v and w for $i = 1$, 2 and 3 respectively
$\bar{u}_i$	time-averaged values of u, v and w
u'_i	velocity fluctuations for components u, v and w
v	y-component velocity
β	frequency parameter
ε	turbulent dissipation
κ	von Karman constant
θ	separation angle
ρ	fluid density
Δ	the averaged grid size
μ	laminar dynamic viscosity
μ_t	eddy viscosity
ν_t	turbulent kinematic viscosity
y^+	non-dimensional distance
τ_{ij}	Reynolds stress tensor or SGS stress term

REFERENCES

1. Tritton DJ. Experiments on the flow past a circular cylinder at low Reynolds numbers. *Journal of Fluid Mechanics* 1959; **6**(4): 547.
2. Achenbach E. Distribution of local pressure and skin friction around a circular cylinder in cross-flow up to $Re = 5 \times 10^6$. *Journal of Fluid Mechanics* 1968; **34**: 625–639.
3. Majumdar S, Rodi W. Numerical calculation of turbulent flow past circular cylinder. In *Proceedings of the 3rd Symposium on Physical Aspects of Aerodynamic Flows*, Long Beach, CA, 1985; pp. 3.13–3.25.
4. Franke R, Rodi W, Schonung B. Analysis of experimental vortex shedding data with respect to turbulence modelling. In *Proceedings of the 7th Turbulent Shear Flow Symposium*, Stanford, USA, 1989; pp. 24.4.1–24.4.5.
5. Cantwell B, Coles D. An experimental study of entrainment and transport in the turbulent near wake of a circular cylinder. *Journal of Fluid Mechanics* 1983; **139**: 321–374.
6. Launder BE, Spalding DB. *Mathematical Models of Turbulence*. Academic Press: London, 1972.
7. Speziale CG. On non-linear k–l and k–ε models of turbulence. *Journal of Fluid Mechanics* 1987; **178**: 459–475.
8. Rabbit MJ. Some validation of standard modified and non-linear k–ε turbulence models. *International Journal for Numerical Methods in Fluids* 1997; **24**: 965–986.
9. Charles CSS, Mingshun Y. Simulation of vortex shedding flow about a circular cylinder a high Reynolds numbers. *Journal of Fluids Engineering* 1990; **112**: 155–163.
10. Zhang J, Dalton C. Interactions of vortex induced vibrations of a circular cylinder and a steady approach flow at a Reynolds number of 13,000. *Computers and Fluids* 1996; **25**(3): 283–294.
11. Kato C, Ikegawa M. Large eddy simulation of unsteady turbulent wake of a circular cylinder using the finite element method. *Advances in Numerical Simulation of Turbulent Flows*, *ASME FED* 1991; **117**: 49–58.

12. Simpson BA, Holdo AE, Byrne CEI. Large eddy simulation of high aspect jets. In *Proceedings of the 2nd International Symposium on Turbulence Heat and Mass Transfer*, Hanjalic J, Peeters T (eds). Delft University Press, 1997.
13. Fluid Dynamics International. *Fidap User Manuals*. FDI: Lebanon, NH, 1993.
14. Yakhot V, Orszag SA, Thangham S, Gatski TB, Speziale CG. Development of turbulence models for shear flows by a double expansion technique. *Physics of Fluids* 1992; **4**(7): 1510–1520.
15. Launder BE. *Lecture Notes on Turbulence Modelling in Industrial Flows*. LES Houches Summer School on Computational Fluid Dynamics, 1993.
16. Smagorinsky J. General circulation experiments with the primitive equations. *Monthly Weather Review* 1963; **91**: 99–152.
17. Prandtl L. Uber ein ausdebildete turbulenz. *Mathematik Mechanics* 1925; **3**: 136–139.
18. Wakes SJ, Holdo AE. Wall functions used with current turbulence models. In *Proceedings of the ASME Fluids Engineering Division*, *Summer Meeting*, Vancouver, 1997.
19. Rodi W, Ferziger JH, Breuer M, Pourquie M. Status of large eddy simulation: results of a workshop. *Transactions of the ASME of Fluids Engineering* 1997; **119**: 248–262.
20. van Driest ER. On turbulent flow near a wall. *Journal of Aerospace Science* 1956; **23**(11): 1007–1011.
21. Bouard R, Coutanceau M. The early state of development of the wake behind and impulsively started cylinder for $40 < Re < 10^4$. *Journal of Fluid Mechanics* 1980; **101**(3): 583–607.

